Reverse Protonation Is the Key to General Acid−Base Catalysis in Enolase[†,‡]

Paul A. Sims, Todd M. Larsen, Russell R. Poyner, W. Wallace Cleland, and George H. Reed*

Department of Biochemistry, University of Wisconsin−Madison, Madison, Wisconsin 53726

Received April 22, 2003; Revised Manuscript Received May 19, 2003

ABSTRACT: The pH dependence of enolase catalysis was studied to understand how enolase is able to utilize both general acid and general base catalysis in each direction of the reaction at near-neutral pHs. Wild-type enolase from yeast was assayed in the dehydration reaction (2-phospho-D-glycerate → phosphoenolpyruvate + H_2O) at different pHs. E211Q, a site-specific variant of enolase that catalyzes the exchange of the α-proton of 2-phospho-D-glycerate but not the complete dehydration, was assayed in a $^1H/^2H$ exchange reaction at different pDs. Additionally, crystal structures of E211Q and E168Q were obtained at 2.0 and 1.8 Å resolution, respectively. Analysis of the pH profile of k_{cat}/K_{Mg} for wild-type enolase yielded macroscopic pK_a estimates of 7.4 ± 0.3 and 9.0 ± 0.3, while the results of the pD profile of the exchange reaction of E211Q led to a pK_a estimate of 9.5 ± 0.1. These values permit estimates of the four microscopic pK_as that describe the four relevant protonation states of the acid/base catalytic groups in the active site. The analysis indicates that the dehydration reaction is catalyzed by a small fraction of enzyme that is reverse-protonated (i.e., Lys345−NH_2, Glu211−COOH), whereas the hydration reaction is catalyzed by a larger fraction of the enzyme that is typically protonated (i.e., Lys345−NH_3^+, Glu211−COO^-). These two forms of the enzyme coexist in a constant, pH-independent ratio. The structures of E211Q and E168Q both show virtually identical folds and active-site architectures (as compared to wild-type enolase) and thus provide additional support to the conclusions reported herein. Other enzymes that require both general acid and general base catalysis likely require reverse protonation of catalytic groups in one direction of the reaction.

Enolase (EC: 4.2.1.11, 2-phospho-D-glycerate hydrolase), an enzyme of glycolysis and gluconeogenesis, catalyzes the interconversion of 2-PGA[1] and PEP according to the kinetic mechanism shown on the following page (*1*).

This mechanism is supported by binding and kinetic data that show a bell-shaped activation curve for divalent metal-ion concentration with an optimum of two divalent metal ions per active site (*2*) and kinetic-isotope-effects data that reveal an approach to unity of V_H/V_D at high magnesium-ion concentrations (*1*). The distinction between E and E′ in the above mechanism is made clear by consideration of the following chemical mechanism that focuses on changes in the above central complexes [i.e., (E-Mg-2-PGA-Mg) and (E′-Mg-PEP-Mg)] (*3*, *4*):

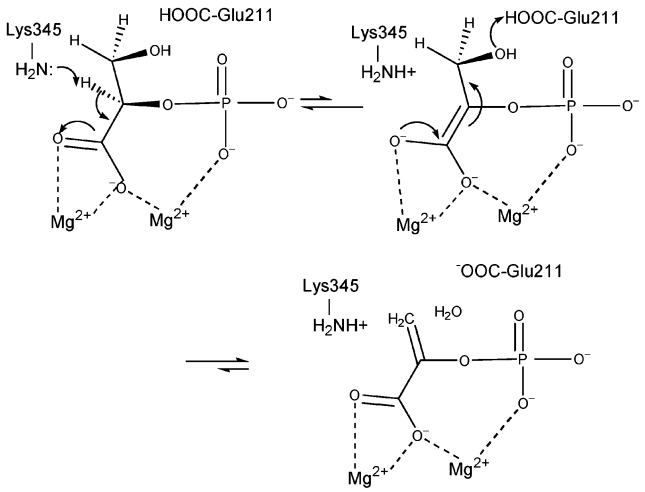

This chemical mechanism is supported by stereochemical data that indicate anti-elimination of H_2O (*5*); isotope-exchange data that demonstrate the presence of a discrete intermediate in the reaction (*6*); site-directed mutagenesis studies that implicate the ϵ-amino moiety of Lys345 and the γ-carboxyl of Glu211 as the catalytic base/acid pair (*3*); and X-ray crystallography data that corroborate the assignment of the side chain functional groups of Lys345 and Glu211 as the catalytic base/acid pair (*7*).

† This research was supported in part by NIH Grants GM35752 (G.H.R.) and GM18938 (W.W.C.).

‡ The atomic coordinates of two enolase variants, E211Q and E168Q, have been deposited with the Protein Data Bank: 1P48 for E211Q and 1P43 for E168Q.

* Address correspondence to the following author. Telephone: (608) 262-0509. Fax: (608) 265-2904. E-mail: reed@biochem.wisc.edu.

[1] Abbreviations: 2-PGA, 2-phospho-D-glycerate; PEP, phosphoenolpyruvate; V_H/V_D, velocity of reaction with protonated substrate (α-proton) over velocity of reaction with deuterated substrate (α-deuteron); DEAE, diethylaminoethyl; CM, carboxymethyl; SDS−PAGE, sodium dodecyl sulfate polyacrylamide gel electrophoresis; MES, 2-(*N*-morpholino)ethanesulfonic acid; HEPES, *N*-(2-hydroxyethyl)piperazine-*N*′-2-ethanesulfonic acid; HEPPS, *N*-(2-hydroxyethyl)piperazine-*N*′-3-propanesulfonic acid; PEG, poly(ethylene glycol); TRIS, Tris(hydroxymethyl)aminomethane; TAPS, *N*-Tris(hydroxymethyl)methyl-3-aminopropanesulfonic acid; CHES, 2-(*N*-cyclohexylamino)ethanesulfonic acid; CAPS, 3-(cyclohexylamino)-1-propanesulfonic acid; NMR, nuclear magnetic resonance; r^2, coefficient of determination (also the explained variation divided by the total variation); rms, root-mean-squared.

10.1021/bi0346345 CCC: $25.00
Published on Web 06/18/2003

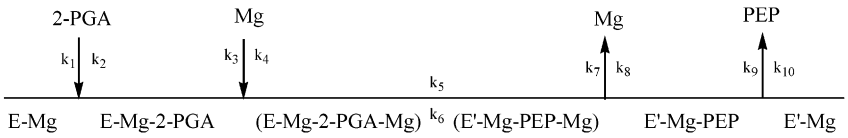

The above chemical mechanism portrays the catalytic residues as being differently protonated at the start and finish of the reaction. Thus, a neutral amino group of Lys345 and a neutral carboxyl of Glu211 (E mentioned above) are required for catalysis in the dehydration reaction, whereas a positively charged ammonium of Lys345 and a negatively charged carboxylate of Glu211 (E′) are required for catalysis in the hydration reaction. Other enzymes that start and finish the catalytic cycle with catalytic groups in altered states of ionization (e.g., those with *Iso* mechanisms) have been discussed previously (*8*).

The proposed mechanism exemplifies what is known as reverse protonation (*9*). This hypothesis, which is applicable for enzymes that use both general acid and general base catalysis in a given direction, holds that differently protonated forms of an enzyme will coexist in reasonable proportions, near the pH optimum, if the microscopic pK_as of the catalytic groups are less than ~2 units apart. One of these enzyme forms will be protonated in a manner opposite (or reverse) from what one would expect given the pK_as of the free amino acids that comprise the catalytic groups in question. The fraction of the reverse-protonated form is determined by the microscopic pK_as of the catalytic groups. Because pH profiles provide information on macroscopic pK_as, additional approaches, as outlined below, are required to gain insight into the microscopic values. Some examples of enzymes that use reverse protonation include malic enzyme (*10*), 6-phosphonogluconate dehydrogenase (*11*), thermolysin (*12*), glycosidase (*13*), carboxypeptidase (*14*), phosphomannomutase/phosphoglucomutase (*15*), and β-xylosidase (*16*). Proline racemase also could be considered to show reverse protonation because one of the catalytic cysteines must be protonated in one direction of the reaction and deprotonated in the other direction (and vice versa for the other catalytic cysteine) (*17*).

The present investigation was undertaken to determine the pH dependence of enolase catalysis and to test further the assignments of catalytic function to groups comprising the active site. Specifically, the pH dependence of the dehydration reaction was studied by use of a systematic variation of both [2-PGA] and [Mg^{2+}] in nonchelating buffer solutions. The information obtained from these pH profiles was complemented with results from a study of the $^1H/^2H$ exchange reaction of 2-PGA catalyzed by E211Q, a site-specific variant of enolase. In addition, structures of both E211Q and E168Q variant forms of enolase were determined at high resolution.

EXPERIMENTAL PROCEDURES

Materials. Enolase from baker's yeast (*Saccharomyces cerevisiae*) was purified as described previously (*18*); however, a polishing column of DEAE-cellulose was used as an additional purification step after the CM-Sephadex column. The conditions for the final DEAE chromatography step (pH 8.0, 20 mM TRIS) were such that enolase did not bind to the resin, but additional contaminants (as judged by SDS−PAGE) did bind. The E211Q and E168Q variants of enolase were expressed recombinantly in *Escherichia coli* and purified as described previously (*3*), except that a final DEAE-cellulose column also was used as described above. The substrates 2-PGA and PEP and the buffers CAPS, TAPS, and CHES were purchased from Sigma. MES and HEPPS buffers were purchased from Research Organics; TRIS and HEPES buffers were purchased from Fisher. Chelex 100 resin was purchased from Bio-Rad. D_2O (99.9 atom % D) and high purity $MgCl_2$ (99.99%) were purchased from Aldrich. PEG 8000 was purchased from Fluka.

Removal of Contaminating Metal Ions. Enolase and 2-PGA solutions were passed through 1 × 5 cm columns of Chelex 100 (200−400 mesh) in the K^+ form to remove contaminating metal ions. In a similar fashion, buffer solutions that were used in the pH and pD profiles were passed through 2.5 × 30 cm or 1 × 5 cm columns of Chelex 100 (200−400 mesh) K^+ form, with the pH or pD of each Chelex 100 column adjusted to match that of the buffer solution.

Standardization of Stock Solutions. Enolase concentrations were determined from absorbance data collected at 280 nm; an extinction coefficient of 0.89 mL mg^{-1} cm^{-1} (*19*) and a subunit molecular weight of 46 500 (*20*, *21*) were used for these determinations. PEP and 2-PGA concentrations were determined by enzymatic end-point assays as described previously (*1*).

Correction for the Change in Extinction Coefficient of PEP. Absorbance data (in triplicate) were collected at 240 nm on stock solutions of PEP that were titrated with increasing [Mg^{2+}] and at different pHs such that kinetic-assay conditions were closely matched. The absorbance data from pH 5.9, 7.5, 8.0, and 9.5 were fitted with PSI-Plot (Poly Software International) to an expression that reflects the change in extinction coefficient of PEP with varying pH and [Mg^{2+}]. This expression, based on Scheme 1, is given in eq 1.

$$\epsilon_{obs} = \frac{\epsilon_{PEP} + \epsilon_{HPEP}H/K_1 + \epsilon_{MgPEP}Mg/K_3}{1 + H/K_1 + Mg/K_3} \qquad (1)$$

The variables in eq 1 are as follows: ϵ_{PEP}, ϵ_{HPEP}, and ϵ_{MgPEP} are the extinction coefficients of PEP^{3-}, $HPEP^{2-}$, and $MgPEP^-$, respectively, *H* represents the concentration of hydrogen ions, and K_1 and K_3 are equilibrium dissociation constants depicted in Scheme 1. This equation, which includes the assumption that free Mg ≈ total Mg, was derived in a manner analogous to a previous expression that related the dependence of the extinction coefficient of PEP to pH

Scheme 1

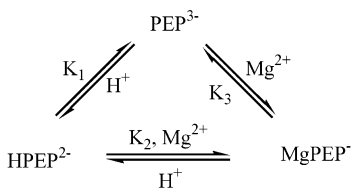

(*22*). Ratios of very small numbers (e.g., H/K_1) were treated as powers of 10 (e.g., $10^{(pK_1-pH)}$) to avoid algorithmic problems of estimating such ratios. Additionally, the literature value of $pK_1 = 6.35$ (*22*) was used for the fit to eq 1. The statistical parameter, r^2, which represents the proportion of total variance explained by the model equation (*23*), was calculated to assess the quality of the fits.

Kinetic Measurements of the Dehydration Reaction. Kinetic assays, done at 25 °C, were conducted such that both [2-PGA] and [Mg^{2+}] were varied systematically and in triplicate at each of the following buffer/pH combinations: MES (pH 5.9 and 6.6); HEPES (pH 7.0, 7.5, and 8.0); TAPS (pH 8.4 and 9.0); and CHES (pH 9.5). Buffers were chosen on the basis of low metal-binding ability (*24*). Typical assay conditions included 0.05 M buffer, 0.02−0.7 mM 2-PGA, 0.03 mM to 0.11 M $MgCl_2$, and 0.01 μM wild-type enolase. (Control assays had zero $MgCl_2$.) The above components, minus enzyme, were mixed thoroughly in quartz cuvettes that had been rinsed in 1 N HCl and absolute EtOH. The mixtures were blanked, enzyme was added, and kinetic data were obtained by monitoring the increase in absorbance of the reaction mixtures at 240 nm as a function of time. This increase in absorbance corresponded to net PEP formation.

The kinetic data were corrected for the change in extinction coefficient of PEP at varying pH and [Mg^{2+}] according to parameters determined from the fit to eq 1. Kinetic data collected at each pH were fitted to eq 2, which reflects the kinetic mechanism (*1*, *25*).

$$v/E_t = \frac{k_{cat}AMg}{K_{ia}K_{Mg} + K_{Mg}A + K_aMg + AMg(1 + Mg/K_i)} \quad (2)$$

The parameters in eq 2 represent a slight modification of the nomenclature of Cleland (*26*) and are as follows: v is the velocity of the reaction, E_t is the total concentration of enzyme, k_{cat} is the turnover number, A is 2-PGA concentration, Mg is magnesium-ion concentration, K_{ia} is the dissociation constant for 2-PGA, K_{Mg} is the Michaelis constant for magnesium, K_a is the Michaelis constant for 2-PGA, and K_i is the inhibition constant for magnesium. Kinetic data obtained with 0.03−10 mM $MgCl_2$ (0.03−55 mM $MgCl_2$ for data collected at pH 5.9) allowed a reasonably symmetric sampling of the activation and inhibition limbs of v/E_t versus log [$MgCl_2$] profiles and were used to estimate k_{cat}, k_{cat}/K_{Mg}, and k_{cat}/K_a (i.e., k_{cat}/K_{2-PGA}). Kinetic data obtained with 0.03 mM to 0.11 M $MgCl_2$ were used to determine K_i. Parameters such as k_{cat}/K_{Mg} were treated as single variables to obtain reliable estimates of errors of these parameters. Samples that matched the reaction conditions were checked to verify that the pH matched that of the buffer; the only variations noted were in samples that contained 0.06 and 0.11 M $MgCl_2$, where the pH of the reaction mixture was consistently lower than that of the buffer by 0.05 and 0.1 units, respectively.

Parameter estimates from eq 2 were plotted as functions of pH according to eqs 3−6 (*9*, *27*):

$$\log\left(\frac{k_{cat}}{K_{Mg}}\right)_{app} = \log\left(\frac{(k_{cat}/K_{Mg})}{(1 + H/K_1 + K_2/H)(1 + H/K')}\right) \quad (3)$$

$$\log\left(\frac{k_{cat}}{K_a}\right)_{app} = \log\left(\frac{(k_{cat}/K_a)}{(1 + K_2/H)}\right) \quad (4)$$

$$\log(k_{cat})_{app} = \log\left(\frac{k_{cat}}{(1 + H/K_{e1} + K_{e2}/H)}\right) \quad (5)$$

$$pK_{i\,app} = pK_i + \log\left(\frac{(1 + K_2/H)}{(1 + H/K_1)}\right) \quad (6)$$

In these equations, app signifies apparent, H represents the concentration of hydrogen ions, K_1 and K_2 represent macroscopic ionization constants of titratable groups on the enzyme, K' represents the ionization constant of 2-PGA, and K_{e1} and K_{e2} represent macroscopic ionization constants of titratable groups on the enzyme in the presence of saturating 2-PGA and Mg^{2+}.

Because the kinetic mechanism of enolase is not perfectly ordered, the kinetic data from 0.03 mM to 0.11 M $MgCl_2$ also were fitted to eq 7, which allows for hyperbolic substrate inhibition (*28*).

$$v/E_t = \frac{k_{cat}AMg}{K_{ia}K_{Mg} + K_{Mg}A + K_aMg + AMg\dfrac{(1 + Mg/K_{in})}{(1 + Mg/K_{id})}} \quad (7)$$

The definitions of parameters in eq 7 are the same as in eq 2 except that K_i is replaced by two constants, K_{in} and K_{id}.

Kinetic Measurements of the Exchange Reaction. E211Q enolase catalyzes the exchange of the α-proton of 2-PGA with protons or deuterons of the solvent, but this variant is ineffective in catalysis of the dehydration of 2-PGA (*3*). This exchange reaction was assayed in D_2O by ^1H NMR spectroscopy at varying pD and included the isotopic correction that pD = pH meter reading + 0.4 (*29*). For these assays, the following buffer/pD combinations were used: 2-PGA (pD 6.2, 6.6, 7.2, 7.5, and 8.0) and CHES (pD 8.5, 9.0, 9.4, 10.1, and 10.5). The assays, done in triplicate, included 0.05 M CHES (for pDs 8.5 and above), 30 mM 2-PGA, 2 mM $MgCl_2$, and 0.8 μM to 0.3 mM E211Q. (The enzyme was diluted at higher pDs to keep the time frames of the assays similar.) The above components, minus E211Q, were mixed thoroughly, and reference spectra were obtained with a 200 MHz NMR spectrometer. Enzyme was added, and additional spectra (each an average of 16 scans) were recorded at suitable intervals as exchange of the α-proton proceeded. This exchange was followed on the basis of changes in the proton NMR spectrum of 2-PGA upon substitution of ^2H for ^1H at the α-carbon as described previously (*3*). The pD of each sample was measured at the conclusion of each assay. The rate and exchange constants for the reaction were determined by fitting the data to eqs 8 and 9, while $\log(k_{ex})_{app}$ was plotted as a function of pD according to eq 10:

$$f = ae^{-kt} \quad (8)$$

$$k_{ex} = k\frac{[2 - PGA]}{[E211Q]} \quad (9)$$

$$\log(k_{ex})_{app} = \log\left(\frac{k_{ex}}{(1 + D/K)}\right) \quad (10)$$

In these equations, f represents the fraction of the NMR signal from the α-proton of 2-PGA, D represents the concentration of deuterium ions, and *K* represents the macroscopic ionization constant of a titratable group on the enzyme in the presence of saturating concentrations of 2-PGA.

Crystallization and Data Collection. Crystals of both E211Q and E168Q were grown by the batch method from solutions containing 10 mg mL^{-1} enzyme, 13% PEG 8000, 0.25 M KCl, 25 mM HEPPS/KOH, pH 8.0, 3.5 mM PEP, and 3.5 mM $MgCl_2$. Microseeding from crystals of the enolase variant S39A was used to initiate crystal growth. Rodlike crystals ~0.1 × 0.2 × 0.5 mm^3 grew within 3 days.

A single crystal of each enolase variant was transferred into a solution (solution A) that contained 50 mM HEPPS/KOH, pH 8.0, 20% PEG 8000, 0.3 M KCl, 5 mM $MgCl_2$, and 4 mM PEP. Each crystal was allowed to equilibrate in solution A for 3 min prior to a five-step serial transfer into solutions that contained increasing concentrations (4% per step) of the cryoprotectant ethylene glycol. The equilibration time between each of the five successive steps was 5 s. After the last serial transfer, each crystal was flash-frozen and stored in liquid nitrogen until data acquisition.

X-ray data were collected with a Bruker Nonius FR591 rotation-anode generator, Montel optics, and a Bruker Proteum R 4K CCD detector. The data set was integrated with the program SAINT (Bruker Nonius) and scaled with ProScale (Bruker Nonius).

Crystals of E168Q (as a complex with Mg^{2+} and 2-PGA) belonged to the space group $P2_12_12$, contained one dimer per asymmetric unit, and had unit cell dimensions a =107.3 Å, b = 115.1 Å, and c = 73.4 Å. The structure of the E168Q complex was solved by molecular replacement using the software program MOLREP from the CCP4 suite (*30*). The search-model coordinates used were from the dimer of the published wild-type enolase structure (*7*). The initial *R* factor was 36.6%. Further refinement of the E168Q structure (from 30 to 1.8 Å resolution) was obtained through use of the software program CNS (*31*). After two cycles of CNS, the overall *R* factor was lowered to 26.7%. Observation of the structure with the graphics program TURBO (*32*) revealed that the conformations of residues 38−40, 156−161, and 265−271, which comprise three active-site loops, required adjustments. These residues were removed, and another two cycles of refinement were executed. The $F_o - F_c$ density maps were then used to rebuild the removed residues. Density corresponding to 2-PGA was clearly present in both subunits. After inclusion of the 2-PGA and both Mg^{2+} ions in each subunit, the water pick algorithm in the CNS package was used to find the positions of ordered water molecules. TURBO was used to make manual adjustments and to include additional water molecules. The final refinement data are given in Table 1.

Crystals of E211Q (as a complex with Mg^{2+} and PEP) belonged to the space group $P2_12_12$, contained one dimer per asymmetric unit, and had unit cell dimensions a =107.8 Å, b = 114.5 Å, and c = 73.1 Å. Initial phases of the E211Q complex were calculated from the refined coordinates of the E168Q structure (minus the 2-PGA, Mg^{2+} ions, and water molecules). After two cycles of CNS, the overall *R* factor was lowered to 26.5%. Observation of the structure with TURBO revealed that the conformations of residues 38−40 and 158−161 in two of the active-site loops required adjustments. The residues in these regions were removed, and two cycles of refinement were executed. The residues were rebuilt using the $F_o - F_c$ density maps. Density corresponding to PEP was clearly present in both subunits. After inclusion of PEP and both Mg^{2+} ions in each subunit, the water pick algorithm in the CNS package and TURBO were used to include additional water molecules and to make manual adjustments. The final refinement data are given in Table 1.

Table 1: Crystal and Refinement Data of the E211Q-Mg^{2+}-PEP Complex and the E168Q- Mg^{2+}-2-PGA Complex

crystallographic data	E211Q	E168Q
space group	$P2_12_12$	$P2_12_12$
cell dimensions (Å)	a = 107.8	a =107.3
	b = 114.5	b = 115.1
	c = 73.1	c = 72.4
no. of measurements	231529	303129
no. of independent reflections	61265	83994
data range (Å)	30−2.0	30−1.8
completeness (%)		
overall	99.0	99.0
last shell	(2.09−2.00) 99	(1.88−1.80) 99
R merge (%)		
overall	6.4	4.7
last shell	18.9	21.7
refinement statistics		
R cryst (%)	18.5	18.5
R factor (free) 5% data (%)	21.3	21.3
rmsd of bonds (Å)	0.0057	0.0050
rmsd of angles (deg)	1.2	1.2
no. of water molecules	743	867

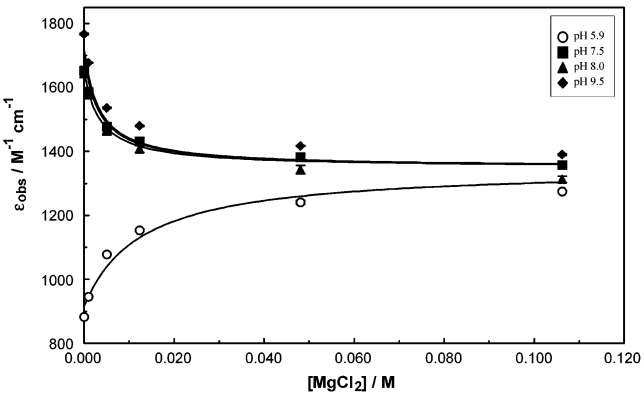

FIGURE 1: Change in extinction coefficient of PEP as a function of [$MgCl_2$] and pH. The lines represent the best fit of the data collected at pH 5.9, 7.5, 8.0, and 9.5 to eq 1 (r^2 = 0.98). The symbols represent means ± one standard deviation.

RESULTS AND DISCUSSION

Change in Extinction Coefficient of PEP. The change in extinction coefficient of PEP at varying pH and [$MgCl_2$], as expressed by eq 1, was best estimated from absorbance data collected at pH 5.9, 7.5, 8.0, and 9.5 (r^2 = 0.98; Figure 1). These data led to the following parameter estimates: ϵ_{PEP} = 1.7 × 10^3 M^{-1} cm^{-1}, ϵ_{HPEP} = 6.3 × 10^2 M^{-1} cm^{-1}, ϵ_{MgPEP} = 1.4 × 10^3 M^{-1} cm^{-1}, and K_3 = 3.3 × 10^{-3} M. These estimates led to predicted values of the extinction coefficient that closely matched the absorbance data from all of the pHs tested (i.e., none of the experimental data, at any of the pHs tested, differed from predicted values by more than 5%; the absolute mean of these deviations was 2%). Accordingly,

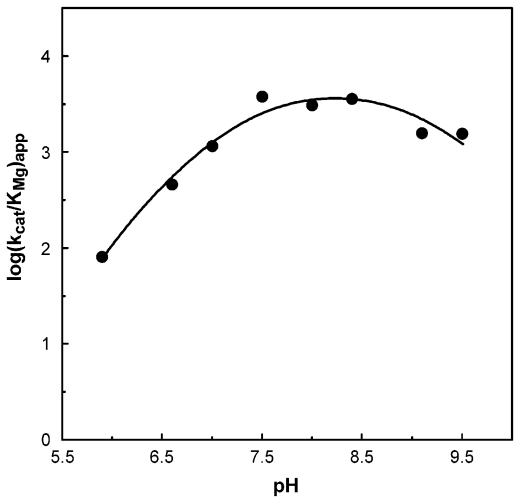

FIGURE 2: pH dependence of $\log(k_{cat}/K_{Mg})$ for wild-type enolase. The line represents the best fit of the data to eq 3 ($r^2 = 0.97$).

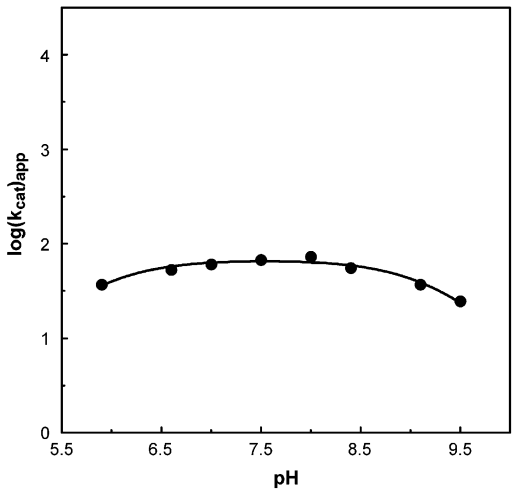

FIGURE 3: pH dependence of $\log(k_{cat})$ for wild-type enolase. The line represents the best fit of the data to eq 4 ($r^2 = 0.96$).

the kinetic data were corrected by use of eq 1 and the above parameter estimates.

pH Dependence of the Forward (Dehydration) Reaction. The pH dependence of $\log(k_{cat}/K_{Mg})_{app}$ is shown in Figure 2. The r^2 for this fit was 0.97, and parameter estimates for pK_1 and pK_2, which correspond to macroscopic ionization constants of titratable groups on the enzyme, were 7.4 ± 0.3 and 9.0 ± 0.3, respectively. The parameter estimate for pK', which corresponds to the ionization constant of 2-PGA, was 5.83 ± 0.55. This estimate is not close to the pK_a of 7.0 that is reported for 2-PGA that is free in solution (*22*), but close agreement was not expected because k_{cat}/K_{Mg} data extrapolate to saturating (and thus bound) 2-PGA and near-zero levels of the second Mg^{2+} (*33*). (The first Mg^{2+} binds with a K_d of 12 nM (*2*) and is considered part of the enzyme.) The pK' estimate is close to the value of 5.82 ± 0.05 that was reported for ionization of 2-PGA when 2-PGA is part of the E-Mg-2-PGA complex (*34*). The latter value of 5.82 corresponds to a microscopic pK_a and was determined from ^{31}P chemical shifts of the 2-PGA in the E-Mg-2-PGA complex as a function of pH (*34*). When the $\log(k_{cat}/K_{Mg})_{app}$ data were refitted to eq 3 such that the ionization constant K' was held fixed at the value of $10^{-5.82}$, the parameter estimates for pK_1 and pK_2 remained the same (as expected), but the standard deviations decreased from ±0.3 to ±0.1 log units.

The estimates of 7.4 for pK_1 and 5.8 for pK' are within experimental error of previous estimates of 7.5 and 6.0 (*25*); however, this previous study did not explicitly identify either of these estimates as being due to ionization of 2-PGA. This earlier study (*25*) also did not extend above pH 8.0 (for this particular profile) so that no estimate for pK_2 is available with which to compare the current estimate. A second study, conducted at a pH range of 5.4−9.25, determined estimates of 5.93 ± 0.93 and 8.39 ± 0.03 (*34*). In fact, the pH profiles of this second study (*34*) and those in the present study differ with respect to many of the pK_a estimates. The apparent discrepancies are likely due to differences in experimental approaches used in the two studies. In the present study, concentrations of both 2-PGA and Mg^{2+} were varied systematically at each pH, and the kinetic data so obtained were fitted to eq 2, which reflects the established kinetic mechanism. The other study (*34*) used either (*1*) varying Mg^{2+} and saturating 2-PGA; (*2*) optimal Mg^{2+} and varying 2-PGA; or (*3*) inhibitory Mg^{2+} and varying 2-PGA. Kinetic data that were obtained from each of the above conditions were fitted either to the Michaelis−Menten equation or to the modified Michaelis−Menten equation that treats uncompetitive inhibition (*34*).

A final point concerning the above profile needs consideration. Namely, how well do the estimates for pK_1 and pK_2 reflect the macroscopic ionizations of the catalytic groups on the enzyme? Since the k_{cat}/K_{Mg} data extrapolate to the form of the enzyme that is poised to combine with the second Mg^{2+} and proceed through catalysis (*33*), this profile should reflect ionizations that are attributable to catalytic groups. Such is not the case with the profile of $\log(k_{cat})_{app}$ versus pH, as will be discussed below.

A plot of $\log(k_{cat})_{app}$ versus pH (Figure 3) shows a broad and somewhat flat profile that curves downward slightly at both ends ($r^2 = 0.96$). The parameter estimates for pK_{e1} and pK_{e2}, which ostensibly represent macroscopic ionization constants of titratable groups on the enzyme in the presence of saturating 2-PGA and Mg^{2+}, were 5.8 ± 0.1 and 9.2 ± 0.1, respectively. A previous study (*34*) reported estimates that ranged from 5.8 to 6.4 for the low-end pK_a and from 8.4 to 8.6 for the high-end pK_a.

As noted, pK_a estimates from pH profiles of $\log(k_{cat})_{app}$ may not correspond to actual ionizations of catalytic groups on the enzyme and may, in fact, be regarded as limiting values (*33*, *35*). The reason these estimates may not reflect actual ionizations is that the parameter k_{cat} (or V) may be comprised of constants that show different pH dependences (*33*, *35*). The extent to which the pH dependences of the constants differ (e.g., the catalytic step versus product release) will determine the closeness of the pK_a estimates to the actual values (*33*). In the case of enolase, the parameter k_{cat} is comprised of constants for both the catalytic step and for product release. A second reason to suspect that the pK_a estimates of 5.8 and 9.2 (obtained from $\log(k_{cat})_{app}$ versus pH) might not reflect ionizations of catalytic groups is that too great a separation in macroscopic pK_as would suggest that one of the catalytic forms of the enzyme would make up too small a fraction of the total enzyme and would not be able to support catalysis at established rates (see below).

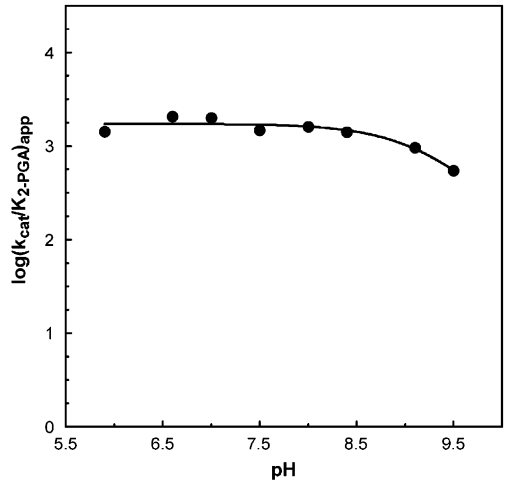

FIGURE 4: pH dependence of $\log(k_{cat}/K_{2-PGA})$ for wild-type enolase. The line represents the best fit of the data to eq 5 ($r^2 = 0.91$).

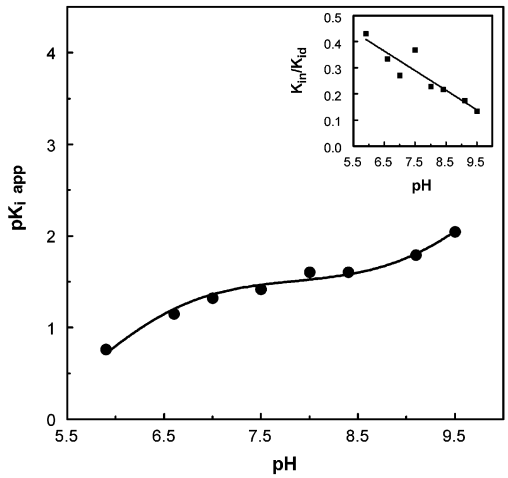

FIGURE 5: pH dependence of the inhibition of wild-type enolase by Mg^{2+}. The line represents the best fit of the data to eq 6 ($r^2 = 0.99$). The inset shows the decline in the ratio of K_{in}/K_{id} as a function of pH ($r = 0.92$). Estimates for K_{in} and K_{id} were determined by fitting the kinetic data to eq 7, which allows for hyperbolic substrate inhibition. The decline in the ratio of K_{in}/K_{id} indicates a more ordered mechanism.

The pH dependence of $\log(k_{cat}/K_{2\text{-}PGA})_{app}$ is shown in Figure 4. This profile is flat at low and intermediate pHs but decreases at high pH. The r^2 for this fit was 0.91, and the parameter estimate for the single pK_a was 9.2 ± 0.1. This pK_a likely reflects ionization of a residue that is important for binding 2-PGA because the k_{cat}/K_{2-PGA} data essentially reflect the productive collision between 2-PGA and enzyme at low levels of 2-PGA and saturating Mg^{2+} (*33*).

A plot of the inhibition constant for Mg^{2+} (in the form of p$K_{i\ app}$) versus pH (Figure 5) breaks downward below a pK_a of 6.6 ± 0.1 and breaks upward above a pK_a of 9.1 ± 0.1 ($r^2 = 0.99$). Because plots of pK_i (for metal-ion activators) versus pH can potentially provide information on ligands of the metals (*36*), the pK_a of 6.6 may reflect ionization of one of the phosphoryl oxygens of 2-PGA/PEP because none of the other ligands to the second Mg^{2+}, as determined by X-ray crystallography (*7*), appears to be a likely candidate. This macroscopic pK_a estimate is higher than either of the microscopic pK_as reported for 2-PGA or PEP, 5.82 and 6.16, respectively (*34*), but this increase may be due in part to contributions from other active-site residues. A net decrease

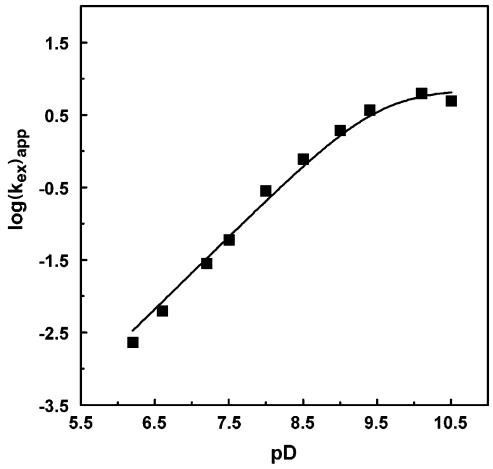

FIGURE 6: pD dependence of the exchange of the α-proton of 2-PGA with solvent deuterons as catalyzed by E211Q. The line represents the best fit of the data to eq 10 ($r^2 = 0.99$).

in positive charge on the enzyme, as would occur at higher pH, should lead to enhanced binding of the second Mg^{2+} (i.e., more efficient inhibition) and thus would explain the increase in pK_i above the second pK_a estimate. The wavelike shape of the profile in Figure 5 differs dramatically from the bell-shaped profile obtained previously by other workers (*34*), probably owing to the different experimental protocols as noted above.

The inset in Figure 5 shows a decline in the ratio of K_{in}/K_{id} as a function of pH ($r = 0.92$). This ratio, which provides a measure of how ordered the reaction is (*1*), was determined by fitting the kinetic data to eq 7, which allows for hyperbolic inhibition (*28*). The decline in the ratio of K_{in}/K_{id} indicates that the mechanism becomes more ordered at higher pH. This interpretation is consistent with the proposal that the second Mg^{2+} becomes a more effective inhibitor at higher pH.

pD Dependence of the $^1H/^2H$ Exchange Reaction of 2-PGA. The pD dependence of the $^1H/^2H$ exchange reaction (exchange of solvent deuterons with the α-proton of 2-PGA), as catalyzed by E211Q enolase, is shown in Figure 6. The r^2 for this fit was 0.99, and the pK_a estimate was 9.5 ± 0.1. The increase in the rate of the exchange reaction at increasing pD is consistent with the hypothesis of reverse protonation because the proportion of enzyme having a neutral ϵ-amino of Lys345 should increase at higher pDs. An increase in the proportion of the enzyme that can function in general base catalysis should lead to an increase in activity, which is observed. In these exchange experiments using the E211Q form of enolase, behavior due to possible ionization of the carboxylate of Glu211 in the active site is eliminated. Thus, while this pK_a is determined from a macroscopic measurement, it is safe to assign this value to the ionization of Lys345. Consequently, the pK_a of 9.0 ± 0.3, obtained from the profile of log k_{cat}/K_{Mg} versus pH for wild-type enzyme, is most logically associated with the ionization of the ϵ-amino of Lys345. The fact that k_{ex} of E211Q is smaller than k_{cat} of wild-type enolase makes it unlikely that release of 2-PGA limits or contributes significantly to k_{ex}. Thus, the pK_a, while not a true microscopic pK_a, provides an approximation of the pK_a for the ϵ-amino of Lys345. A previous study used an analogous approach to estimate the microscopic pK_as of lysozyme (*37*). The authors of this previous study (*37*) esterified Asp52, one of the general base/acid groups of the

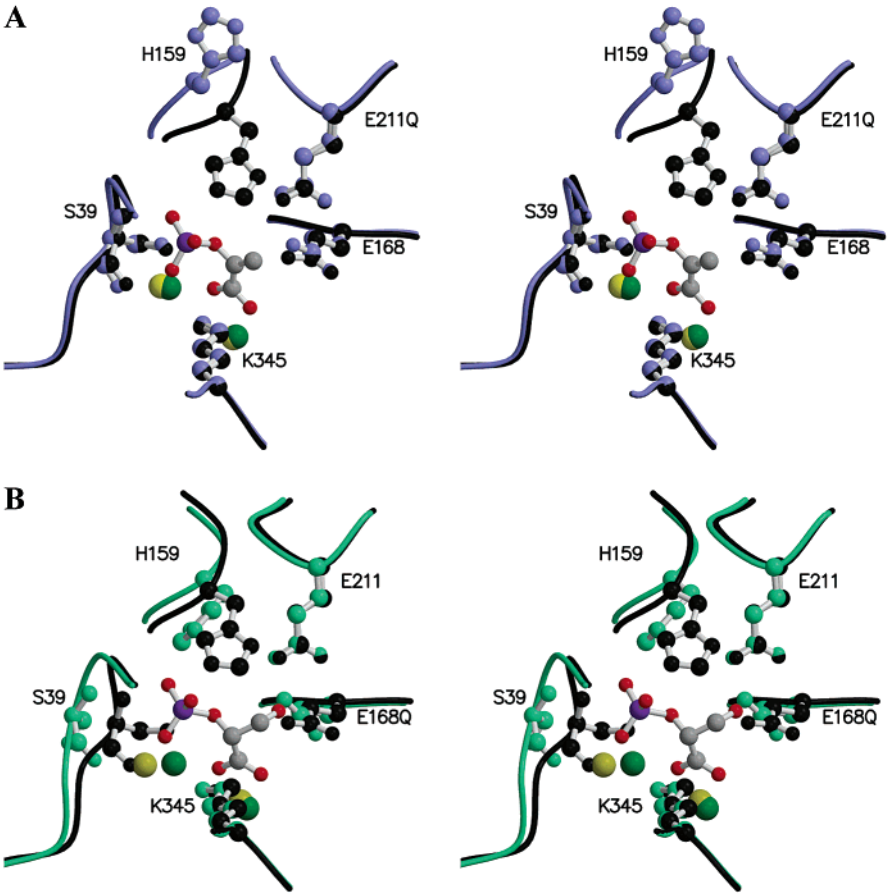

FIGURE 7: (A) Stereoview of the active site of E211Q (light-blue residues, yellow magnesium ions) overlaid against wild-type enolase (black residues, dark-green magnesium ions; obtained from PDB entry code 1ONE; ref *7*). (B) Stereoview of the active site of E168Q (light green) overlaid against wild-type enolase as in panel A. The program MOLSCRIPT (*45*) was used to prepare this figure.

enzyme, and performed difference titrations to obtain estimates of the microscopic ionization constants.

Crystal Structures. The overall folds of both E211Q and E168Q are similar to those of wild-type enolase. The rms deviation between the C-α-carbons of wild-type enolase (*7*) and those of E211Q was 0.59 Å, with a maximum deviation of 3.14 Å (His159). When residues from the three active-site loops were removed (#s 38−42, 155−164, and 251−279), the rms displacement decreased to 0.36 Å, and the maximum deviation dropped to 1.4 Å (Gly202). The rms deviation between the C-α-carbons of wild-type enolase (*7*) and those of E168Q was 0.86 Å, with a maximum displacement of 4.6 Å (Gly161). Removal of the same loop residues as above decreased the rms deviation to 0.31 Å and dropped the maximum displacement to 1.8 Å (Gln219).

A stereoview of the active sites of E211Q and E168Q (both overlaid with wild-type enolase; ref *7*) shows that the catalytic residues Lys345 and Glu/Gln211 are essentially unchanged (Figure 7). Also, Glu/Gln168 shows little change with respect to wild-type enolase. The position of Ser39 in the E211Q structure (Figure 7A) is similar to that seen in wild-type enolase but in the E168Q structure (Figure 7B), Ser39 is positioned farther out from the substrate than is Ser39 of wild-type enolase. The position of His159 in the E211Q structure (Figure 7A) is splayed upward as compared to the same residue in wild-type enolase. His159 in the E168Q structure is similarly positioned with His159 of the wild-type structure, but the orientation of the imidazole rings is different (Figure 7B). The two magnesium ions in the E211Q structure show little movement as compared to the magnesium ions in the structure of wild-type enolase (Figure 7A), but Mg438 in the E168Q structure (Figure 7B) is positioned away from Mg438 of the wild-type structure. The altered position of Mg438 in the E168Q structure can be rationalized on the basis of the altered position of Ser39, which coordinates Mg438 with its carbonyl oxygen and γ-oxygen.

None of the above changes are dramatic or surprising given that both Ser39 and His159 form parts of flexible loops so some movement is expected. The observation that the variant structures are properly folded suggests that the altered activity of these variants, especially that of E211Q, is not due to misfolding. Interestingly, all of the E211Q subunits contained PEP, whereas all of the E168Q subunits contained 2-PGA. Since both proteins were cocrystallized with PEP, the E168Q variant must have catalyzed the hydration of PEP.

Case for Reverse Protonation. Enzymes that use general acid−base catalysis, especially those in which one group on the enzyme functions as the general-acid catalyst and a second group functions as the general-base catalyst (with the roles switched for the reverse reaction), can often be modeled as shown in Scheme 2 (*35*, *38*). Thus, a doubly protonated form (HEH) can, upon loss of a proton, give rise to either HE or EH, the two singly protonated forms. (For this example, EH is the typically protonated form, and HE is the reverse-protonated form.) Loss of a second proton then

Scheme 2

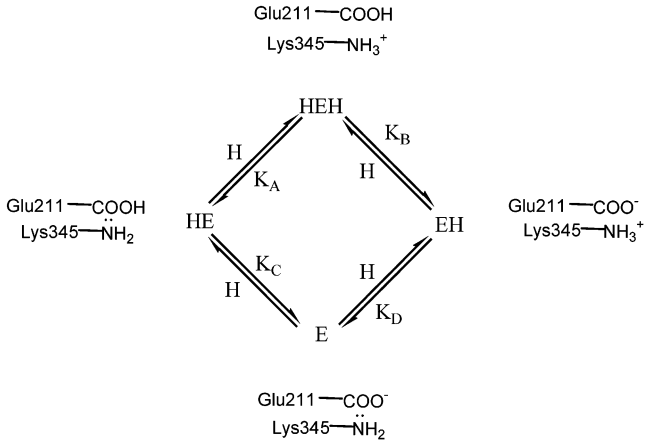

gives rise to E, the unprotonated form. The equations that express the relationships among the different forms of enzyme of Scheme 2 are given in eqs 11−17.

$$K_1 = K_A + K_B \tag{11}$$

$$K_2 = \frac{K_C K_D}{(K_C + K_D)} \tag{12}$$

$$K_A K_C = K_B K_D = K_1 K_2 \tag{13}$$

$$\frac{HEH}{E_t} = \frac{1}{(1 + K_1/H + K_1K_2/H^2)} \tag{14}$$

$$\frac{HE}{E_t} = \frac{1}{(1 + H/K_A + K_B/K_A + K_C/H)} = \frac{1}{(1 + H/K_A + K_C/K_D + K_C/H)} \tag{15}$$

$$\frac{EH}{E_t} = \frac{1}{(1 + H/K_B + K_A/K_B + K_D/H)} = \frac{1}{(1 + H/K_B + K_D/K_C + K_D/H)} \tag{16}$$

$$\frac{E}{E_t} = \frac{1}{(1 + H/K_2 + H^2/K_1K_2)} \tag{17}$$

The parameters in eqs 11−17 are as follows: K_1 and K_2 represent macroscopic ionization constants; K_A, K_B, K_C, and K_D represent microscopic ionization constants; H represents the concentration of hydrogen ions; and E_t represents the total concentration of enzyme.

Inspection of Scheme 2 and/or of eqs 11−17 shows that at least one of the microscopic ionization constants must be known (in addition to the macroscopic ionization constants K_1 and K_2) to determine the proportion of enzyme form that is either HE or EH. If the pK_a estimate of 9.5 from the ^{1}H/^{2}H exchange assay is used to approximate the microscopic ionization constant K_A of Scheme 2, then estimates of the proportions of all the enzyme forms become possible. Given this assumption, $K_A \approx 10^{-9.5}$, $K_B \approx 10^{-7.4}$, $K_C \approx 10^{-6.9}$, and $K_D \approx 10^{-9}$. The pK_as attributable to Glu211 (e.g., 7.4 and 6.9) are high as compared to the value of 4.1 that is assigned to the γ-carboxyl of free glutamate. There is, however, precedent for elevated pK_as of side chains of Glu residues that are positioned in the active sites of enzymes (*39*, *40*). In the case of enolase, the proximity of Glu168 to Glu211 (Figure 7) likely perturbs the pK_a of Glu211 upward. The approximate nature of these assignments is indicated by the observation that $K_A < K_D$ and $K_B < K_C$, which is inconsistent with the model represented by Scheme 2. Nonetheless, the above assignments allow one to construct a plot of enzyme form as a function of pH (Figure 8), and this plot should provide a reasonable framework in which to interpret enolase catalysis.

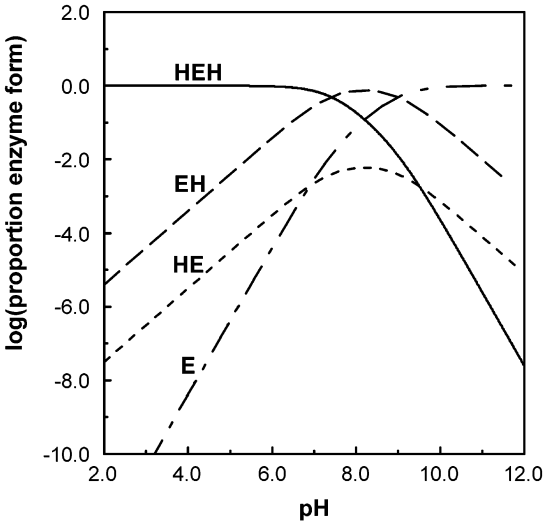

FIGURE 8: Proportion of enzyme form as a function of pH. HEH represents the doubly protonated form; EH represents the typically protonated form; HE represents the reverse-protonated form; and E represents the unprotonated form.

A striking feature of Figure 8 is that even at the pH optimum of 8.2, a significant proportion of the enzyme exists as the doubly protonated form HEH and as the unprotonated form E (12% each). The typically protonated form EH accounts for 75% of the enzyme form. Thus, very little (~1%) of the reverse-protonated form HE is available for catalysis in the dehydration reaction. In fact, when the accepted k_{cat}/K_m value (80 $s^{-1}/5 \times 10^{-5}$ M) is corrected for the fraction of enzyme that is HE, the result (3×10^8 M^{-1} s^{-1}) is within an order of magnitude of the diffusion-controlled limit. A separation of macroscopic pK_as (and therefore, microscopic pK_as) that is greater than about 2 units would leave too small a fraction of the reverse-protonated form to catalyze the reaction.

Given the above constraints on the separation of pK_as, one might ask why Lys345 was selected to act as a base in the dehydration reaction? Why do enzymes not use residues with more closely matched pK_as such that more equitable distributions of enzyme forms result? A possible answer comes from Marcus theory (*41*) as applied to α-proton abstraction from carbon acids (*42*, *43*). The rate of this type of reaction is related to the ΔpK_a (separation in pK_as between the general-base catalyst of the enzyme and the α-proton of the substrate) by eq 18 (*42*, *43*).

$$k = \left(\frac{k_B T}{h}\right)\exp\{-[(\Delta G^{\ddagger}/RT) + \beta_e 2.303\Delta pK_a]\} \tag{18}$$

The variables in eq 18 are as follows: k is the rate of proton

abstraction; k_B is Boltzmann's constant; T is the absolute temperature; h is Planck's constant; $\Delta G^{\ddagger}$ is the intrinsic barrier to isoergonic proton transfer; R is the gas constant; and β_e is the Brønsted coefficient for base-catalyzed enolization of the carbon acid. The use of Lys345 as a base allows a smaller ΔpK_a than would occur with a different residue that has a lower pK_a. For example, the rate of proton abstraction is 10−100 times faster (depending on the β_e) with an enzyme base that has a pK_a of 9 versus one that has a pK_a of 7. Similar observations concerning general acid−base catalysis by RNA were made recently (*44*). Thus, the penalty of having a small fraction of the enzyme in an active form can potentially be offset by a kinetic advantage. Consequently, natural selection would not be expected a priori to select for more equitable distributions of enzyme forms, and additional explanations for the "choice" of Lys345 and Glu211 must be sought. Perhaps a greater proportion of the typically protonated form EH is required for catalysis because hydration of the double bond between α- and β-carbons of PEP is a more difficult first step than is abstraction of the α-proton of 2-PGA in the dehydration reaction. Theoretical calculations in this area may provide additional insight into this intriguing question.

ACKNOWLEDGMENT

We are grateful to Drs. Matthew M. Benning and Cary Bauer for assistance. We thank Prof. Perry A. Frey for a helpful discussion on why reverse protonation occurs and Mr. Steve Monsoorabadi for helpful discussions on rate equations and the distributions of enzyme forms.

REFERENCES

1. Poyner, R. R., Cleland, W. W., and Reed, G. H. (2001) *Biochemistry 40*, 8009−8017.
2. Faller, L. D., Baroudy, B. M., Johnson, A. M., and Ewall, R. X. (1977) *Biochemistry 16*, 3864−3869.
3. Poyner, R. R., Laughlin, L. T., Sowa, G. A., and Reed, G. H. (1996) *Biochemistry 35*, 1692−1699.
4. Reed, G. H., Poyner, R. R., Larsen, T. M., Wedekind, J. E., and Rayment, I. (1996) *Curr. Opin. Struct. Biol. 6*, 736−743.
5. Cohn, M., Pearson, J. E., O'Connell, E. L., and Rose, I. (1970) *J. Am. Chem. Soc. 92*, 4095−4098.
6. Dinovo, E. C., and Boyer, P. D. (1971) *J. Biol. Chem. 246*, 4586−4593.
7. Larsen, T. M., Wedekind, J. E., Rayment, I., and Reed, G. H. (1996) *Biochemistry 35*, 4349−4358.
8. Rebholz, K. L., and Northrop, D. B. (1995) *Methods Enzymol. 249*, 211−240.
9. Cleland, W. W. (1977) *Adv. Enzymol. 45*, 273−387.
10. Nuiry, I. I., and Cook, P. F. (1985) *Biochim. Biophys. Acta 829*, 295−298.
11. Price, N. E., and Cook, P. F. (1996) *Arch. Biochem. Biophys. 336*, 215−223.
12. Mock, W. L., and Stanford, D. J. (1996) *Biochemistry 35*, 7369−7377.
13. Joshi, M. D., Sidhu, G., Pot, I., Brayer, G. D., Withers, S. G., and McIntosh, L. P. (2000) *J. Mol. Biol. 299*, 255−279.
14. Mock, W. L., and Cheng, H. (2000) *Biochemistry 39*, 13945−13952.
15. Naught, L. E., and Tipton, P. A. (2001) *Arch. Biochem. Biophys. 396*, 111−118.
16. Vocadlo, D. J., Wicki, J., Rupitz, K., and Withers, S. G. (2002) *Biochemistry 41*, 9736−9746.
17. Albery, W. J., and Knowles, J. R. (1986) *Biochemistry 25*, 2572−2577.
18. Wedekind, J. E., Poyner, R. R., Reed, G. H., and Rayment, I. (1994) *Biochemistry 33*, 9333−9342.
19. Warburg, O., and Christian, W. (1941) *Biochem. Z. 310*, 384−421.
20. Chin, C. C., Brewer, J. M., and Wold, F. (1981) *J. Biol. Chem. 256*, 1377−1384.
21. Holland, M. J., Holland, J. P., Thill, G. P., and Jackson, K. A. (1981) *J. Biol. Chem. 256*, 1385−1395.
22. Wold, F., and Ballou, C. E. (1957) *J. Biol. Chem. 227*, 301−312.
23. *PSI-Plot, Version 7* (2002) Poly Software International, New York.
24. Good, N. E., Winget, G. D., Winter, W., Connolly, T. N., Izawa, S., and Singh, R. M. M. (1966) *Biochemistry 5*, 467−477.
25. Anderson, V. E. (1981) Ph.D. Thesis, University of Wisconsin−Madison, Madison, WI.
26. Cleland, W. W. (1963) *Biochim. Biophys. Acta 67*, 104−137.
27. Segel, I. H. (1975) in *Enzyme Kinetics: Behavior and Analysis of Rapid Equilibrium and Steady-State Enzyme Systems*; John Wiley & Sons, Inc., New York.
28. Cleland, W. W. (1963) *Biochim. Biophys. Acta 67*, 173−187.
29. Glasoe, P. K., and Long, F. A. (1960) *J. Am. Chem. Soc. 64*, 188−190.
30. Vagin, A., and Teplyakov, A. (1997) *J. Appl. Crystallogr. 30*, 1022−1025.
31. Brunger, A. T. (1998) *Acta Crystallogr. D54*, 905−921.
32. Roussel, A., and Cambillau, C. (1991) in *Silicon Graphics Geometry Partners Directory*, Silicon Graphics, Mountain View, CA.
33. Cleland, W. W. (1970) Steady-state kinetics, in *The Enzymes* (Boyer, P. D., Ed.) pp 1−65, Academic Press, New York.
34. Vinarov, D. A., and Nowak, T. (1998) *Biochemistry 37*, 15238−15246.
35. Kyte, J. (1995) in *Mechanism in Protein Chemistry*, Garland Publishing, Inc., New York.
36. Cleland, W. W. (1982) *Methods Enzymol. 87*, 390−405.
37. Parsons, S. M., and Raftery, M. A. (1972) *Biochemistry 11*, 1623−1629.
38. Cornish-Bowden, A. (1976) in *Principles of Enzyme Kinetics*, Butterworth & Co., Boston.
39. Fersht, A. (1999) in *Structure and Mechanism in Protein Science*, W. H. Freeman & Co., New York.
40. Joshi, M. D., Sidhu, G., Nielsen, J. E., Brayer, G. D., Withers, S. G., and McIntosh, L. P. (2001) *Biochemistry 40*, 10115−10139.
41. Marcus, R. A. (1968) *J. Phys. Chem. 72*, 891−899.
42. Gerlt, J. A., Kozarich, J. W., Kenyon, G. L., and Gassman, P. G. (1991) *J. Am. Chem. Soc. 113*, 9667−9669.
43. Gerlt, J. A., and Gassman, P. G. (1992) *J. Am. Chem. Soc. 114*, 5928−5934.
44. Bevilacqua, P. C. (2003) *Biochemistry 42*, 2259−2265.
45. Kraulis, P. J. (1991) *J. Appl. Crystallogr. 24*, 946−950.

BI0346345